

Received July 19, 2019, accepted August 11, 2019, date of publication August 14, 2019, date of current version August 28, 2019.

Digital Object Identifier 10.1109/ACCESS.2019.2935310

330-500 GHz Graphene-Based Single-Stage High-Order Subharmonic Mixer

ANDREEA IOANNA HADARIG, SAMUEL VER HOEYE¹, (Member, IEEE), MIGUEL FERNÁNDEZ¹, CARLOS VÁZQUEZ¹, LETICIA ALONSO¹, (Student Member, IEEE), AND FERNANDO LAS-HERAS¹, (Senior Member, IEEE)

Department of Electrical Engineering, University of Oviedo, 33203 Gijón, Spain

Corresponding author: Miguel Fernández (fernandezgmiguel@uniovi.es)

This work was supported in part by the European Union Seventh Framework Programme (FP/2007-2013) under Project 600849, in part by the Spanish Agencia Estatal de Investigación (AEI) and Fondo Europeo de Desarrollo Regional (FEDER) under Project TEC2016-80815-P (AEI/FEDER, UE) and Project TEC2015-72110-EXP (AEI), and in part by the Gobierno del Principado de Asturias (PCTI) and FEDER under Project IDI/2016/000372, Project IDI/2017/000083, and Project IDI/2018/000191.

ABSTRACT In this work, a graphene-based single-stage high-order subharmonic mixer is presented. The device is able to up- and downconvert a signal in the 330–500 GHz frequency range, using a local oscillator signal with frequency located in the 26–40 GHz band. It exploits the strong nonlinear electromagnetic behavior exhibited by macroscopic graphene sheets when they are exposed to an incident electromagnetic wave to generate the output signal as a mixing product between the input signal and a high-order harmonic component of the local oscillator, which is internally generated without requiring additional circuitry. A prototype was implemented and its performance was experimentally characterized considering several different local oscillator multiplication orders. The maximum measured downconversion gain is around –50 dB, whereas the maximum output signal reached when working as upconverter is –43 dBm at 340 GHz and –63 dBm at 480 GHz. These values are good enough to be used in practical short-range applications. Furthermore, the measurement results are in good agreement with the theoretical predictions about graphene behavior.

INDEX TERMS Electromagnetic modeling, frequency conversion, graphene, subharmonic mixer, submillimeter wave technology.

I. INTRODUCTION

The development of electronic devices working in the submillimeter wave frequency band is presently attracting a considerable research effort. Due to the non-harmful nature and the particular penetration characteristics of electromagnetic radiation in that frequency band, a continuously increasing number of electromagnetic imaging applications in fields as diverse as medical diagnosis [1]–[4], pharmaceuticals [5], security [6], non-destructive material testing [7], or analysis of artworks [8], [9] is being proposed.

Nowadays, the most common approach to generate and detect signals in the submillimeter wave band involves the use of Schottky diodes [10] to implement frequency multipliers [11]–[16] and subharmonic mixers [17]–[21]. Because of the low efficiency of Schottky diodes when

generating harmonic components with order greater than 2 or 3, and with the exception of some recently developed single-stage quadrupler designs [15], [16], the frequency multipliers and the local oscillator chain of subharmonic mixers are usually composed of several low-order multiplying stages [20], [22], [23], generally requiring the use of inter-stage components, such as power amplifiers and isolators. Although this technology represent the state-of-art, the high economic cost derived from the complexity of the required topologies and the involved manufacturing processes, specially when working at frequencies near the THz band, limits the practical development of commercial applications.

During the last decade, the scientific community has paid a great attention to graphene. Due to its unique properties, a very large number of applications have been found in a wide variety of scientific and technical fields. Regarding the design of frequency mixers, several works describing the use of

The associate editor coordinating the review of this article and approving it for publication was Yuhao Liu.

graphene-based diodes [24], [25], and graphene Field Effect Transistors (GFET) [26]–[31] in integrated MMIC designs have been reported, with promising results. The main drawback of this approach is the fact that the maximum working frequency of GFETs is strongly conditioned by their maximum oscillation frequency $f_{max} \approx 40$ GHz, limiting their use as active devices to the microwave band. Nevertheless, the use of GFET to implement subharmonic mixers [32]–[35] and signal detectors [36], [37] working in the submillimeter wave band has also been described. In this case, resistive mixer implementations are usually used to overcome the f_{max} limitation, showing that they are able to downconvert RF signals at frequencies up to $f_{RF} = 400$ GHz. However, the use of a low multiplication value in the local oscillator (LO) chain implies the use of a very high frequency input local oscillator signal to provide a moderate intermediate frequency (IF).

On the other hand, a radically new generation of submillimeter wave signal generators and detectors based on the use of macroscopic graphene sheets instead of GFETs or Schottky diodes has been developed in the last few years. This technology allows the implementation of single-stage high-order frequency multipliers [38], [39], [41] and subharmonic mixers [42], [43], which exploit the nonlinear electromagnetic behavior exhibited by graphene layers exposed to an incident electromagnetic field to generate high-order harmonic components in the case of the multipliers, and mixing products in the case of the mixers. Regarding the frequency multipliers, devices covering the 140 – 220 GHz [8], 220 – 330 GHz [38]–[40], and 330 – 500 GHz [41] bands have been described, whereas subharmonic mixers capable of downconverting RF signals in the 140 – 220 GHz [8] and 220–330 GHz [42], [43] bands have also been reported. Both the multiplier input and the mixer local oscillator signals are located in the K_a band (26–40 GHz). The performance of this technology is noticeably far from the state-of-art represented by Schottky diode based devices, but the use of easily obtainable graphene layers combined with a single-stage topology allows a drastic reduction of the economic cost, since the only additional external device is an amplifier working in the K_a band, and no MMIC implementation techniques are required. Furthermore, it has been demonstrated that the proposed frequency multipliers and mixers provide output power and conversion gain values that are good enough to be used in practical submillimeter wave transmitters [44], receivers [45], [46], and imaging systems [8], [9].

In this work, a graphene-based single-stage high-order subharmonic mixer working in the 330 and 500 GHz, and capable of performing up- and downconversion operations, is presented. The input LO signal is located in the 26–40 GHz band, and the intermediate frequency f_{IF} is around 400 MHz. The device performance in terms of downconversion gain and maximum output power will be experimentally characterized. The presented device provides a low-cost solution to detect and to generate signal in the 330 – 500 GHz band, with a performance good enough to be used in cost-effective short-range applications. To the best knowledge of the authors,

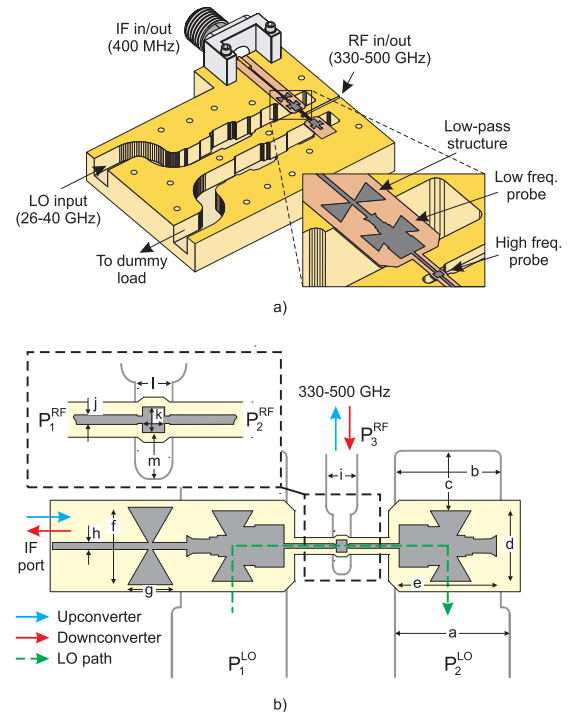


FIGURE 1. (a) Section view of the mixer. The inset shows details of the planar circuit around the transitions. (b) Planar circuit. The dark area represents the structured graphene sheet, whereas the light shaded area represents the polyimide substrate.

this is the first time that a graphene-based mixer capable of working with an RF signal in the 330 – 500 GHz is described. Furthermore, the obtained measurement data is in good agreement with the theoretical studies about graphene, which predict that it is able to generate an infinite set of harmonic components of an input signal, with slowly decaying amplitude, and that this effect should be observable at room temperature from the microwave to the low-THz frequency bands [47]–[50].

The paper is organized as follows. In section II, the topology and the working principle are presented. Section III describes the design process, whereas some implementation details are provided in section IV. Section V is devoted to the in-depth experimental characterization. Finally, the obtained results are discussed in section VI.

II. TOPOLOGY AND WORKING PRINCIPLE

A. TOPOLOGY

Because of the advantages of the topology proposed in [42], in terms of cost and ease of implementation, the proposed device presents a similar structure, which is schematized in Fig. 1 (a). The main dimensions are summarized in Table 1. The device is composed of a planar circuit embedded in a waveguide structure that is used to provide the input and to extract the output signals. The planar circuit is represented in Fig. 1 (b). It is composed of a polyimide substrate film on which a graphene film was transferred, to act as the circuit metallization. The graphene sheet is structured to obtain one

TABLE 1. Value of the main dimensions of the planar circuit, indicated in Fig. 1 (b).

dim.	(mm)	dim.	(mm)	dim.	(mm)	dim.	(mm)
a	3.56	e	3.1	i	0.56	m	0.38
b	3.24	f	2.3	j	0.09		
c	1.82	g	1.42	k	0.16		
d	2.13	h	0.24	l	0.31		

high- and two low-frequency probes that are the planar parts of the planar-to-waveguide transitions. It also includes one low-pass structure to block the leakage of the RF and LO signals towards the IF port. On the other hand, the waveguide structure is composed of two identical WR28 sections to manage the OL signal, one WR2.2 section for the RF signal, and a channel interconnecting them to host the planar circuit. Note that in Fig. 1 (a) only one of the two identical halves obtained from cutting the waveguide block along the E-plane of the waveguides is represented.

The proposed mixer can work as up- and downconverter. In both cases, the local oscillator signal is located in the 26 – 40 GHz frequency band. It is provided to the device through one of the WR28 waveguide sections, and coupled to the planar circuit at the corresponding low-frequency probe, exciting the graphene film. The portion of the LO signal that cannot be converted at the graphene layer is coupled to the second WR28 waveguide section and delivered to a matched load, minimizing in this way the return losses at the LO port over the whole 26 – 40 GHz band without requiring additional components.

B. WORKING PRINCIPLE

It was theoretically predicted [47]–[50] that a graphene sheet exposed to an incident monochromatic electromagnetic wave with angular frequency $\omega = 2\pi f$ generates a current J composed of a theoretically infinite set of odd-order harmonic components with slowly decaying amplitude:

$$J \propto \sum_{n=0}^{\infty} \frac{1}{2n+1} \sin\{(2n+1)\omega t\} \quad (1)$$

From (1), the amplitude of the induced harmonic components does not depend on the magnitude of the input field, provided that it is greater than a certain threshold, which depends on the temperature and working frequency. This effect can be observed at room temperature, from the microwave to the low-THz frequency range [47]. Thus, the bandwidth of a device based in the described phenomenon is virtually only limited by the circuitry surrounding the graphene sheet. The described behavior was experimentally demonstrated using simple topologies capable of working as second- [51]–[54] and third-order [55]–[57] frequency multipliers.

Furthermore, if two signals at different frequencies f_{LO} and f_{RF} , i. e. the LO and the RF signals, respectively, are present in the circuit, the induced current J will also contain mixing products with frequency $f_{mix} = |m \cdot f_{LO} \pm k \cdot f_{RF}|$,

TABLE 2. Approximate f_{LO} values for different multiplication orders. All the values are expressed in GHz.

	$m = 8$	$m = 10$	$m = 12$	$m = 14$	$m = 16$
$f_{RF} = 330$	41.3	33.04	27.54	23.6	-
$f_{RF} = 410$	-	41.04	34.2	29.31	25.65
$f_{RF} = 500$	-	-	41.7	35.74	31.27

with m and k integers [58]–[60]. Since the level of the received RF signal will be, in general, much lower than that of the LO signal, only the terms with $k = 1$ will be observable. In addition, it has to be taken into account that, because of the central symmetry of graphene, and under normal incidence of the driving signal, the amplitude of the odd-order harmonic components of the LO signal (odd m) and that of the mixing products (with even value of m) will be dominant.

When working as downconverter, the RF signal propagates towards the planar circuit along the WR2.2 waveguide section and is coupled to it through the high frequency probe. The output IF signal, with frequency $f_{IF} = 400$ MHz is then obtained as a mixing product between a high-order harmonic component of the LO signal, which is generated at the graphene sheet, and the received RF signal. Hence, its frequency can be expressed as $f_{IF} = f_{RF} - m \cdot f_{LO}$. Since this signal cannot propagate towards any of the waveguide sections, it will be guided to the output IF port.

On the other hand, if the device works as upconverter, the IF signal is provided to the planar circuit at the IF port and mixed with a high-order harmonic component of the LO signal to obtain the RF signal, whose frequency can be expressed as $f_{RF} = m \cdot f_{LO} \pm f_{IF}$. It will be coupled to the WR2.2 waveguide section at the high-frequency transition to be extracted from the device.

The combination of WR28 and WR2.2 rectangular waveguides for the LO and the RF signals, respectively, allows the use of different local oscillator multiplication orders m to downconvert/generate the RF signal. Table 2 shows the approximate LO frequencies required to work with RF signals located in the 330 – 500 GHz range, as a function of the selected value of m . The empty cells are associated to f_{LO} values which are outside the nominal monomode working range of the WR28 standard waveguide (i. e. $\approx 22 - 42$ GHz) and, thus, they should not be used.

III. DESIGN

Because of the unavailability of a graphene model capable of accurately predicting the amplitude of the induced current terms, the main goal of the design procedure is to optimize the frequency response of the device, in order to ensure that the graphene sheet will be properly driven by the LO signal, and that the IF and the RF signals will be efficiently coupled from/to the planar circuit, depending on the working mode.

All the simulations were performed using the commercial *Ansys High-Frequency Structure Simulator* electromagnetic solver, based on the finite element method. The multi-layer

graphene sheet was modeled as a $5 \mu\text{m}$ -thickness layer with parallel and perpendicular conductivity values $\sigma_{\parallel} = 2.1 \cdot 10^6$ and $\sigma_{\perp} = 500 \text{ S/m}$, respectively, provided by the manufacturer. In addition, the Groiss model implemented in the simulation software was used to compute the additional propagation losses in the waveguide sections due to the roughness of their walls [61].

The dimensions of the cross-section of the waveguide segments used to propagate the LO and the RF signals coincide with those of the standards WR28 and WR2.2, respectively. To design the planar circuit, it is divided into three sub-networks associated to the RF, LO, and IF signal paths, as represented in Fig. 1 (b), and the indicated ports are defined. Then, the main parameters are roughly estimated using conventional analytical approaches and, finally, they are optimized through CAD techniques.

A. RF PATH

The RF sub-network includes the region indicated with a dashed-line square in Fig. 1 (b), together with the channel which hosts the planar circuit and the WR2.2 waveguide section. Three ports P_1^{RF} , P_2^{RF} , and P_3^{RF} were defined at the marked points to evaluate its frequency response.

Regarding the behavior in the 330 – 500 GHz range, the goal is to maximize the efficiency of the high-frequency transition. It is achieved by minimizing the value of S_{11}^{RF} and S_{22}^{RF} , and ensuring that the value of $|S_{31}^{RF}|$ is as close to 0 dB as possible, and exhibits flat frequency response along the considered band. The geometrical parameters defining the E-plane rectangular-shaped high-frequency probe and the shape of the WR2.2 waveguide around it were optimized using CAD techniques. Furthermore, the channel cross-section was calculated to have a cut-off frequency above 500 GHz, avoiding in this way the propagation of the involved signals as a waveguide mode. Finally, because of its dimensions, the influence of the high-frequency probe on the LO signal is negligible. The obtained results are represented in Fig. 2 (a). On the one hand, a good performance in terms of matched bandwidth was obtained. On the other hand, the coupling factor from P_1^{RF} or P_2^{RF} to P_3^{RF} exhibits a flat frequency response along the whole frequency range, with a -5 dB value. Note that it takes into account the propagation losses in the planar circuit and in the WR2.2 waveguide section.

B. LO PATH

After designing the RF sub-network, the frequency response of the LO signal path, indicated with a green dashed trace in Fig. 1 (b) is analyzed. In this case, the considered sub-network includes the two WR28 waveguide sections, the two low-frequency transitions, and the previously optimized RF sub-network placed between them. Two reference ports P_1^{LO} and P_2^{LO} , located at the interface with the two WR28 waveguide sections, are defined to evaluate the network performance. Now, the main goal is the optimization of the low-frequency waveguide-to-planar transitions

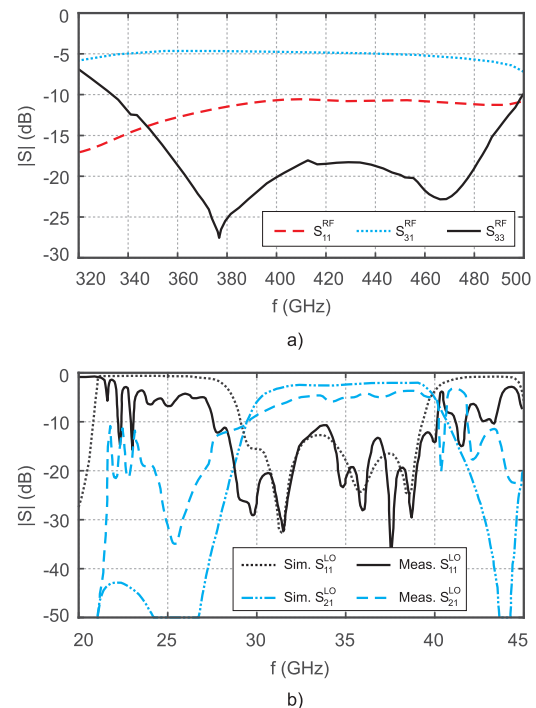


FIGURE 2. Simulated frequency response of the device (a) RF sub-circuit. (b) LO sub-circuit.

to maximize the LO oscillator power coupled to the planar circuit over the 26 – 40 GHz frequency range.

The two identical low-frequency probes are composed of several partially-overlapped triangular-shaped sections. In order to maximize their efficiency, the parameters defining their geometry and that of the waveguide sections around them, as well as the position of the terminating backshorts, were optimized using CAD techniques. Figure 2 (b) shows the obtained results. From the plotted data, a good input impedance matching was achieved between 28 and 39 GHz. The insertion losses in the same frequency band present a flat frequency response, with a value around 4 dB, which can be considered an acceptable performance. At this point, it has been taken into account that this parameter corresponds to the back-to-back connection of the two low-frequency transitions and, thus, includes the losses at the two WR28 waveguide sections and the planar circuit.

Regarding the LO-to-RF leakage, since the frequency of the LO signal is located in the 26 – 40 GHz band, it is below the cut-off frequency of the standard WR2.2 RF waveguide. Therefore, the LO power present at the RF port will be negligible. On the other hand, when working as upconverter, the frequency of the m^{th} harmonic component of the LO signal involved in the mixing operation is very close to that of the RF signal and, thus, it can be coupled to the WR2.2 waveguide together with the RF signal. However, the power of the $m \cdot f_{OL}$ component is considerably lower than that of the RF signal because it is an even-order harmonic component [47]–[50]. In this way, the desired RF signal is hardly distorted.

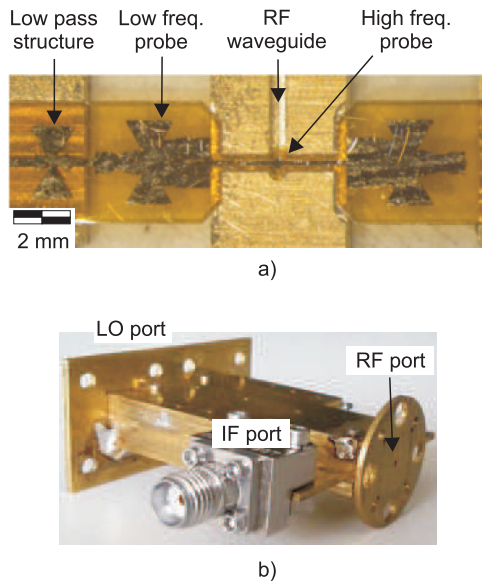


FIGURE 3. Implemented prototype (a) Detail of the planar circuit. (b) General view. Note that the LO ports are in a hidden face.

C. IF PATH

Once the performance of the planar circuit and the waveguide sections is optimized in the 26 – 40 and the 330 – 500 GHz frequency ranges, one low-pass structure was added to the planar circuit. It consists of two parallel triangular stubs, and is located between the IF port and the nearest low-frequency transition. The purpose of this structure is to limit the LO signal leakage through the IF port, and it provides a minimum 17 dB isolation throughout the whole bandwidth of the low-frequency transitions.

IV. IMPLEMENTATION

A prototype of the subharmonic mixer was implemented to validate the proposed design approach.

A. PLANAR CIRCUIT

The graphene sheet used as metallization of the planar circuit was obtained through direct exfoliation from a block of highly-ordered pyrolytic graphite. Then, it was transferred onto a 25 μm polyimide substrate, with dielectric constant $\epsilon_r \approx 3.5$ and loss tangent $\tan\delta = 0.008$. After that, the graphene sheet was structured through a laser ablation process, in order to obtain the desired shape.

B. WAVEGUIDE BLOCK

To obtain the waveguide block, eight 1 mm thickness brass sheets were sequentially micromachined. Then, they were stacked and aligned using several 1 mm diameter screws, and the planar circuit was mounted and fixed to the channel. Standard interface flanges for both the WR28 and the WR2.2 waveguides were separately manufactured and soldered to the waveguide block. Finally, an end-launch SMA-type coaxial connector was mounted at the IF port. Figure 3 shows different details of the manufactured prototype.

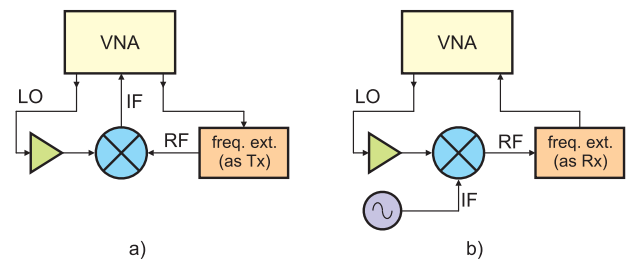


FIGURE 4. Measurement setup. (a) Mixer working as downconverter. (b) Mixer working as upconverter.

V. EXPERIMENTAL CHARACTERIZATION

A. MEASUREMENT SETUP

The prototype was experimentally characterized using the measurement setup schematized in Fig. 4, composed of a vector network analyzer (VNA) and a frequency extender module. The LO signal is generated by the VNA and an amplifier working in the 26 – 45 GHz range. Regarding the behavior as downconverter, the test RF signal is generated by the high-order multiplier chain embedded in the frequency extender module. Due to its frequency response, the RF signal power varies from –15 to –35 dBm along the 330 – 500 GHz range. This power variation was experimentally characterized in order to accurately evaluate the prototype conversion gain. The level of the generated IF signal, at a fixed frequency $f_{IF} = 400$ MHz, is directly evaluated with the VNA.

To evaluate the performance as upconverter, the measurement setup is modified, as indicated in Fig. 4 (b). In this case, the IF signal is provided by a conventional signal generator, and the power of the RF signal generated at the device is measured using the frequency extender module working as receiver.

B. LO-BAND PERFORMANCE

The input impedance matching and the insertion losses of the LO signal path were characterized by connecting both WR28 waveguide terminals to two ports of the VNA, to measure the reflection and the transmission parameters. The obtained results are represented in Fig. 2 (b), together with simulation data. Considering the input impedance matching, the frequency range in which $S_{11} < -10$ dB is extended with respect to the simulation, to be approximately between 28 and 40 GHz. In the case of the insertion losses, the measured value is slightly higher than the simulated one, specially at the lower frequency end. It is probably due to a slight misalignment between the planar circuit and the waveguide block. In addition, when transferring exfoliated graphene sheets onto a flexible substrate, the presence of micro-fissures on the graphene sheet was observed. These defects are also expected to have a negative impact on the overall circuit losses. At any case, since the difference between the simulated and the measured S_{21}^{LO} is below 2 dB, a good mixing performance is expected for f_{LO} between 30 and 40 GHz.

C. PERFORMANCE AS DOWNCONVERTER

The conversion gain is defined as G_c (dB) = P_{IF} (dBm) – P_{RF} (dBm), i. e., the difference between the power values

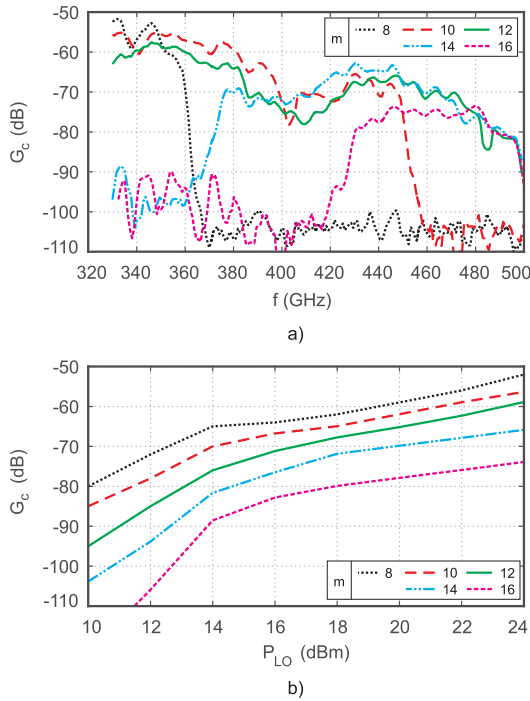


FIGURE 5. (a) Measured maximum conversion gain G_c in downconversion mode, with $P_{LO} = 24$ dBm. (b) Evolution of the maximum conversion gain with P_{LO} .

of the output IF and the input RF signals, P_{IF} and P_{RF} , respectively. It was evaluated for even-order LO multiplication values m between 8 and 16, which provide the IF signal as an odd-order mixing term. Figure 5 (a) represents the evolution of the measured conversion gain along the 330 – 500 GHz band, obtained when the power of the local oscillator is $P_{LO} = 24$ dBm.

First, as was theoretically predicted in [47], the nonlinear electromagnetic behavior of graphene exhibits a flat frequency response from the microwave to the low-THz range. Therefore, the output signal should be generated when the graphene sheet is properly driven, i. e., when the LO frequency, calculated as $f_{LO} = (f_{RF} - f_{IF})/m \approx f_{RF}/m$, is located inside the nominal monomode working range of the WR28 standard waveguide, as indicated in Table 2. However, the cut-off frequency observed in the traces with $m = 8$ and $m = 10$, at $f_{RF} \approx 360$ and 450 GHz, respectively, is due to the amplifier frequency response, whose upper limit is around 45 GHz. In addition, the lower limit of the traces with $m = 14$ and $m = 16$, at $f_{RF} \approx 370$ and 430 GHz, respectively, is imposed by the lowest frequency of the amplifier response, which is about 25.9 GHz. Finally, the observed ripple is due to the combined effects of all the circuitry surrounding the graphene, which includes the frequency responses of the amplifier, the waveguide block and the transitions, specially that of the LO path shown in Fig. 2 (b), and the measurement equipment.

On the other hand, the traces associated with the multiplication orders $m = 10, 12,$ and 14 reveal the existence of a region around 400 GHz in which the conversion gain

sensibly reduces. The effect is observed for different LO multiplication orders and it is located around the same output frequency region, which means that it occurs for very different values of the LO frequency. On the other hand, since the simulation and measurement data relative to the RF and LO signal paths shown in Fig. 2 do not reveal any anomalous behavior, a design error can be discarded. Furthermore, as has been previously stated, the graphene exhibits a flat frequency response along the considered frequency range. Thus, the most likely cause is an unexpected behavior of the implemented high-frequency transition between the planar circuit and the WR2.2 waveguide section, which is probably due to manufacturing issues derived from using exfoliated graphene sheets and a flexible substrate.

Figure 5 (b) represents the evolution of the conversion gain with the local oscillator power, evaluated at the output frequency which provides the maximum value for each LO multiplication order in Fig. 5 (a). The conversion gain increases with P_{LO} , whereas the slope of each trace when $P_{LO} > 14$ dBm is smaller than the expected $m + 1$ value, which indicates that the graphene sheet is saturated. Finally, it was observed that local oscillator power values under 10 dBm did not provide output signal with power greater than the noise floor of the measurement equipment, whereas values higher than 24 dBm were unsafe, since they were near to the power limit that can be managed by the planar circuit.

D. PERFORMANCE AS UPCONVERTER

Regarding the behavior of the prototype as upconverter, the input IF signal, with frequency $f_{IF} = 0.4$ GHz is mixed with the m^{th} -order harmonic component of the LO signal to generate the RF output signal with frequency $f_{RF} = m \cdot f_{LO} + f_{IF}$ located in the 330 – 500 GHz range.

The evolution of the measured upconversion gain $G_{c,up}$ along the 330–500 GHz range, reached with $P_{LO} = 24$ dBm and IF signal power $P_{IF} = 12$ dBm, as a function of the LO multiplication order m , is represented in Fig. 6 (a). Similar considerations about the frequency response as in the downconversion mode can be extracted. On the other hand, the evolution of the output RF signal power with P_{LO} , as a function of m was represented in Fig. 6 (b). As in the downconverter case, the LO power was swept from 10 to 24 dBm, with a 2 dB step.

VI. DISCUSSION

Considering the downconversion performance, from the evolution of the measured conversion gain with the LO power and the LO multiplication order m represented in Fig. 5 (b), it increases with P_{LO} , since the nonlinear electrodynamic response of the graphene is progressively strengthened. The theoretically expected increment rate, i. e., the slope of the characteristic G_c vs. P_{LO} , is $m + 1$. This rate is approximately verified for all the multiplication orders when considering low LO power values, but it tends to saturate for LO power values greater than ≈ 14 dBm, which means that the given graphene sheet is generating the maximum

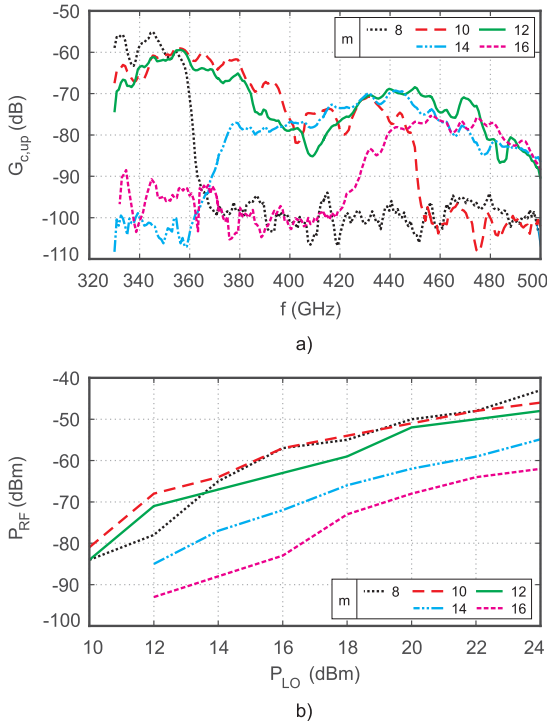


FIGURE 6. (a) Measured maximum conversion gain $G_{c,up}$ in upconversion mode, with $P_{LO} = 24$ dBm. (b) Evolution of the maximum conversion gain with P_{LO} .

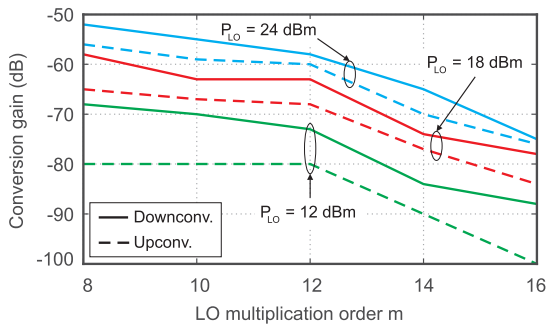


FIGURE 7. Evolution of the measured up- and downconversion gain values with the LO multiplication order m , for three different P_{LO} values.

achievable IF power. Figure 7 represents the variation of the measured up- and downconversion gain with the LO multiplication order, for three different values of P_{LO} . As it is expected from (1), the conversion gain slowly reduces as m increases, which is consistent with the theoretical results reported in [47], [48], and makes possible the practical implementation of single-stage high-order topologies.

Regarding the upconversion mode, the RF output power measurement data shown in Fig. 6 (b) reveals that the maximum reached values with $m = 8, 10$ and 12 are similar for a given P_{LO} , which is consistent with the assumption that the graphene sheet is saturated and, thus, generating the maximum achievable output power. On the other hand, LO multiplication orders $m = 14$ and 16 provide lower output RF level, following the behavior predicted by (1). Figure 8 represents the estimated output RF voltage V_{RF} as a function

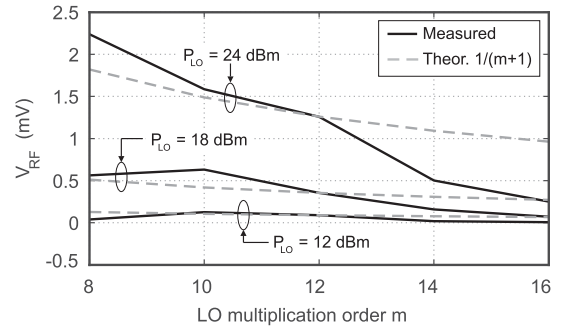


FIGURE 8. Measured output RF voltage V_{RF} as a function of m in upconversion mode, compared with the theoretical evolution $\propto 1/(m+1)$.

of the LO multiplication order m . The values of V_{RF} were derived from the measured output RF power assuming a 50Ω load. The measured output RF voltage exhibits good agreement with the theoretically predicted evolution proportional to $1/(m+1)$, with the exception of the trace corresponding with $P_{LO} = 24$ dBm when considering m values greater than 12 . At any case, it has been taken into account that both, the downconversion gain and the output RF power were measured at different RF frequencies and, thus, they are slightly affected by the variations of the device frequency response.

The evolution of the downconversion gain and the output RF voltage with the mixing order $m+1$ shown in Figs. 7 and 8, respectively, exhibits good agreement with the theoretically predicted electrodynamic response of graphene [47]–[50]. On the one hand, together with the preliminary results presented in [41], it is demonstrated that the nonlinear electromagnetic response of graphene can be experimentally observed, at least, up to 500 GHz at room temperature. On the other hand, the slowly decaying characteristic of the amplitude of the induced harmonic components and mixing terms was experimentally verified. At any case, note that the theoretical electrodynamic behavior of graphene was derived under ideal conditions, considering 2D infinite and isolated graphene layers.

Finally, Table 3 summarizes a performance comparison between the described prototype and other recently reported graphene-based mixers capable of working above 100 GHz. References [32]–[34] describe MMIC circuits based on GFETs. Although they reported good conversion gain values, LO signals with frequency around 100 [33], [34] and 200 GHz [32], and power level between 8 and 16 dBm are used, requiring external high-performance frequency multipliers. On the other hand, works [8] and [42] present subharmonic mixers based on macroscopic graphene sheets, following a design approach similar to that used in this work. When comparing with [32]–[34], the reached conversion gain is considerably reduced, but they use a LO signal located in the $26 - 40$ GHz frequency band which, despite the required power level, is easier to obtain, since the power amplifier technology in the K_a band is well established. This fact, combined with the single-stage topology and the use of simple manufacturing techniques, enables a drastic cost reduction.

TABLE 3. Summarized comparison between the actual device and recently reported graphene-based mixers capable of working above 100 GHz.

Ref.	RF band (GHz)	IF (GHz)	Subharmonic order	P_{LO} (dBm)	Gain (dB)
[32]	185-205	1	1	16	-25
[33]	90-100	1	1	8	-18
[34]	185-215	1	2	12.5	-29
[42]	220-330	0.3	5-14	22	-65
[8]	140-220	0.3	6-10	20	n. a.
This work	330-500	0.4	8-16	24	-52

Furthermore, the measured performance of the actual device is comparable to that reported in [8] and [42], which means that the device can be used as signal detector or generator in practical short-range applications.

VII. CONCLUSION

This work presents a graphene-based single-stage high-order subharmonic mixer working in the 330 – 500 GHz frequency band, with local oscillator in the 26 – 40 GHz range and a 400 MHz intermediate frequency, which is able to work as up- and downconverter. A prototype was implemented and its performance was characterized as a function of the local oscillator power and multiplication order. First, the performance of the implemented prototype, in terms of the down-conversion gain and output RF power, is similar to that of the other previously reported devices which have shown their technical viability to be used in the development of practical short-range applications. On the other hand, the single-stage topology, combined with the use of a relatively low frequency local oscillator signal, and the fact that MMIC technology is not required, enables a drastic cost reduction when comparing with other approaches working in a similar frequency range. Finally, the measurement data is in good agreement with the previously reported theory, which predicts that the nonlinear electromagnetic behavior of graphene is observable from the microwave to the low-THz spectrum region.

REFERENCES

- [1] G. G. Hernandez-Cardoso, S. C. Rojas-Landeros, M. Alfaro-Gomez, A. I. Hernandez-Serrano, I. Salas-Gutierrez, E. Lemus-Bedolla, A. R. Castillo-Guzman, H. L. Lopez-Lemus, and E. Castro-Camus, "Terahertz imaging for early screening of diabetic foot syndrome: A proof of concept," *Sci. Rep.*, vol. 7, Jul. 2017, Art. no. 42124. doi: 10.1038/srep42124.
- [2] F. Dornuf, P. Martín-Mateos, B. Duarte, B. Hils, O. E. Bonilla-Manrique, F. Larcher, P. Acedo, and V. Krozer, "Classification of skin phenotypes caused by diabetes mellitus using complex scattering parameters in the millimeter-wave frequency range," *Sci. Rep.*, vol. 7, Jul. 2017, Art. no. 5822. doi: 10.1038/s41598-017-06034-0.
- [3] P. Martín-Mateos, F. Dornuf, B. Duarte, B. Hils, A. Moreno-Oyervides, O. E. Bonilla-Manrique, F. Larcher, V. Krozer, and P. Acedo, "In-vivo, non-invasive detection of hyperglycemic states in animal models using mm-Wave spectroscopy," *Sci. Rep.*, vol. 6, Sep. 2016, Art. no. 34035. doi: 10.1038/srep34035.
- [4] Z. D. Taylor, R. S. Singh, D. B. Bennett, P. Tewari, C. P. Kealey, N. Bajwa, M. O. Culjat, A. Stojadinovic, H. Lee, J.-P. Hubschman, E. R. Brown, and W. S. Grundfest, "THz medical imaging: In vivo hydration sensing," *IEEE Trans. THz Sci. Technol.*, vol. 1, no. 1, pp. 201–219, Sep. 2011. doi: 10.1109/TTHZ.2011.2159551.
- [5] R. K. May, M. J. Evans, S. Zhonz, C. Byers, L. F. Gladden, Y. Shen, and J. A. Zeidler, "Terahertz pulsed imaging of surface variations on pharmaceutical tablets," in *Proc. 35th Int. Conf. Infr., Millim., THz. Waves*, Rome, Italy, Sep. 2010, pp. 1–2. doi: 10.1109/ICIMW.2010.5612402.
- [6] A. Luukanen, R. Appleby, M. Kemp, and N. Salmon, "Millimeter-wave and terahertz imaging in security applications," *Terahertz Spectrosc. Imag.*, vol. 171, pp. 491–520, Oct. 2012.
- [7] I. Kemp, M. Peterson, C. Benton, and D. T. Petkie, "Sub-mm wave imaging techniques for non-destructive aerospace materials evaluation," in *Proc. IEEE Nat. Aerosp. Electron. Conf. (NAECON)*, Dayton, OH, USA, Jul. 2009, pp. 166–168. doi: 10.1109/NAECON.52009.5426634.
- [8] S. Ver Hoeye, M. Fernández, C. Vázquez, A. I. Hadarig, R. Camblor, L. Alonso, and F. Las-Heras, "Graphene based THz electromagnetic imaging system for the analysis of artworks," *IEEE Access*, vol. 6, pp. 66459–66467, 2018. doi: 10.1109/ACCESS.2018.2879161.
- [9] C. Vázquez, R. Camblor, S. Ver Hoeye, A. Hadarig, G. Hotopan, M. Fernández, and F. Las Heras, "Millimetre wave imaging system for the detection of hidden elements in artwork," in *Proc. Int. Conf. Electromagn. Adv. Appl.*, Palm Beach, The Netherlands, 2014, pp. 675–678. doi: 10.1109/ICEAA.2014.6903943.
- [10] I. Mehdi, J. V. Siles, C. Lee, and E. Schlecht, "THz diode technology: Status, prospects, and applications," *Proc. IEEE*, vol. 105, no. 6, pp. 990–1007, Jun. 2017. doi: 10.1109/JPROC.2017.2650235.
- [11] J. V. Siles, A. Maestrini, B. Alderman, S. Davies, H. Wang, J. Treuttel, E. Leclerc, T. Narhi, and C. Goldstein, "A single-waveguide in-phase power-combined frequency doubler at 190 GHz," *IEEE Microw. Wireless Compon. Lett.*, vol. 21, no. 6, pp. 332–334, Jun. 2011. doi: 10.1109/LMWC.2011.2134080.
- [12] J. Treuttel, L. Gatilova, F. Yang, A. Maestrini, Y. Jin, A. Cavanna, T. Vacelet, F. Tamazouzt, J.-M. Krieg, and C. Goldstein, "A 330 GHz frequency doubler using European MMIC Schottky process based on e-beam lithography," in *Proc. 31st Gen. Assem. Sci. Symp.*, Beijing, China, Aug. 2014, pp. 1–4. doi: 10.1109/URSISGASS.2014.6929454.
- [13] J. V. Siles, K. Cooper, C. Lee, R. Lin, G. Chattopadhyay, and I. Mehdi, "A compact room-temperature 510-560 GHz frequency tripler with 30-mW output power," in *Proc. 15th Eur. Radar Conf.*, Madrid, Spain, Sep. 2018, pp. 333–336. doi: 10.23919/EuRAD.2018.8546537.
- [14] C. Guo, X. Shang, M. J. Lancaster, J. Xu, J. Powell, H. Wang, B. Alderman, and P. G. Huggard, "A 135–150-GHz frequency tripler with waveguide filter matching," *IEEE Trans. Microw. Theory Techn.*, vol. 66, no. 10, pp. 4608–4616, Oct. 2018. doi: 10.1109/TMTT.2018.2855172.
- [15] S. Nadri, L. Xie, M. Jafari, N. Alijbari, M. E. Cyberey, N. S. Barker, A. W. Lichtenberger, and R. M. Weikle, "A 160 GHz frequency quadrupler based on heterogeneous integration of GaAs Schottky diodes onto silicon using SU-8 for epitaxy transfer," in *Proc. IEEE Int. Microw. Symp.*, Philadelphia, PA, USA, Jun. 2018, pp. 769–772. doi: 10.1109/MWSYM.2018.8439536.
- [16] J. Jun, L. Bin, M. Li, H. Yue, S. Xiangyang, T. Yaoling, H. Hailong, C. Fengjung, D. Xianjin, and Z. Jian, "Single-stage frequency quadrupler with SBD and four-octave LPF at 335 GHz," *IEEE Trans. THz Sci. Technol.*, vol. 7, no. 4, pp. 446–454, Jul. 2017. doi: 10.1109/TTHZ.2017.2709720.
- [17] V. Drakinskiy, P. Sobis, H. Zhao, T. Bryllert, and J. Stake, "Terahertz GaAs Schottky diode mixer and multiplier MIC's based on e-beam technology," in *Proc. Int. Conf. Indium Phosph. Rel. Mater. (IPRM)*, Kobe, Japan, May 2013, pp. 1–2. doi: 10.1109/ICIPRM.2013.6562606.
- [18] J. Treuttel, L. Gatilova, A. Maestrini, D. Moro-Melgar, F. Yang, F. Tamazouzt, T. Vacelet, Y. Jin, A. Cavanna, J. Matéos, A. Féret, C. Chaumont, and C. Goldstein, "A 520–620-GHz Schottky receiver front-end for planetary science and remote sensing with 1070 K–1500 K DSB noise temperature at room temperature," *IEEE Trans. THz Sci. Technol.*, vol. 6, no. 1, pp. 148–155, Jan. 2016. doi: 10.1109/TTHZ.2015.2494621.
- [19] P. J. Sobis, N. Wadefalk, A. Emrich, and J. Stake, "A broadband, low noise, integrated 340 GHz Schottky diode receiver," *IEEE Microw. Wireless Compon. Lett.*, vol. 22, no. 7, pp. 366–368, Jul. 2012. doi: 10.1109/LMWC.2012.2202280.
- [20] E. W. Bryerton and J. L. Hesler, "Comparison of Schottky mixer versus low noise amplifier front ends for submillimeter wave receivers," in *Proc. 42nd Int. Conf. Infr., Millim., THz Waves*, Cancun, Mexico, Aug./Sep. 2017, pp. 1–2. doi: 10.1109/IRMMW-THz.2017.8066885.

- [21] A. Maestrini, L. Gatilova, J. Treuttel, Y. Jin, A. Cavanna, D. M. Melgar, T. Vacelet, A. Feret, S. Caroopen, G. Gay, F. Dauplay, J.-M. Krieg, B. Thomas, P. de Maagt, and C. Goldstein, "The 1200 GHz receiver frontend of the submillimetre wave instrument of ESA Jupiter ICy moons explorer," in *Proc. 43rd Int. Conf. Infr., Millim., THz Waves*, Nagoya, Japan, Sep. 2018, pp. 1–2. doi: [10.1109/IRMMW-THz.2018.8509935](https://doi.org/10.1109/IRMMW-THz.2018.8509935).
- [22] T. W. Crowe, J. Hesler, S. Retzlöff, C. Pouzou, and G. Schoenthal, "Solid-state LO sources for greater than 2 THz," in *22nd Space THz Technol. Symp. Dig.*, Apr. 2011, pp. 209–212.
- [23] S.-W. Chang, C.-Y. E. Tong, A. Hedden, Y.-J. Hwang, and R. Blundell, "A 660 GHz local oscillator subsystem: Design, testing and alignment," in *Proc. 39th Eur. Microw. Conf.*, Rome, Italy, Sep./Oct. 2009, pp. 834–837. doi: [10.23919/EUMC.2009.5295970](https://doi.org/10.23919/EUMC.2009.5295970).
- [24] M. Saeed, A. Hamed, Z. Wang, M. Shaygan, D. Neumaier, and R. Negra, "Metal-insulator-graphene diode mixer based on CVD graphene-on-glass," *IEEE Electron Device Lett.*, vol. 39, no. 7, pp. 1104–1107, Jul. 2018. doi: [10.1109/LED.2018.2838451](https://doi.org/10.1109/LED.2018.2838451).
- [25] A. Hamed, M. Saeed, Z. Wang, M. Shaygan, D. Neumaier, and R. Negra, "6–12 GHz MMIC double-balanced upconversion mixer based on graphene diode," in *IEEE MTT-S Int. Microw. Symp. Dig.*, Philadelphia, PA, USA, Jun. 2018, pp. 674–677. doi: [10.1109/MWSYM.2018.8439211](https://doi.org/10.1109/MWSYM.2018.8439211).
- [26] M. Tian, X. Li, Q. Gao, X. Xiong, Z. Zhang, and Y. Wu, "Improvement of conversion loss of resistive mixers using Bernal-stacked bilayer graphene," *IEEE Electron Device Lett.*, vol. 40, no. 2, pp. 325–328, Feb. 2019. doi: [10.1109/LED.2018.2889153](https://doi.org/10.1109/LED.2018.2889153).
- [27] Q. Gao, X. Li, M. Tian, X. Xiong, Z. Zhang, and Y. Wu, "Short-channel graphene mixer with high linearity," *IEEE Electron Device Lett.*, vol. 38, no. 8, pp. 1168–1171, Aug. 2017. doi: [10.1109/LED.2017.2718732](https://doi.org/10.1109/LED.2017.2718732).
- [28] O. Habibpour, J. Vukusic, and J. Stake, "A 30-GHz integrated subharmonic mixer based on a multichannel graphene FET," *IEEE Trans. Microw. Theory Techn.*, vol. 61, no. 2, pp. 841–847, Feb. 2013. doi: [10.1109/TMTT.2012.2236434](https://doi.org/10.1109/TMTT.2012.2236434).
- [29] J. S. Moon, H.-C. Seo, M. Antcliffe, D. Le, C. McGuire, A. Schmitz, L. O. Nyakiti, D. K. Gaskill, P. M. Campbell, K.-M. Lee, and P. Asbeck, "Graphene FETs for zero-bias linear resistive FET mixers," *IEEE Electron Device Lett.*, vol. 34, no. 3, pp. 465–467, Mar. 2013. doi: [10.1109/LED.2012.2236533](https://doi.org/10.1109/LED.2012.2236533).
- [30] M. A. Andersson, O. Habibpour, J. Vukusic, and J. Stake, "Resistive graphene FET subharmonic mixers: Noise and linearity assessment," *IEEE Trans. Microw. Theory Techn.*, vol. 60, no. 12, pp. 4035–4042, Dec. 2012. doi: [10.1109/TMTT.2012.2221141](https://doi.org/10.1109/TMTT.2012.2221141).
- [31] O. Habibpour, S. Cherednichenko, J. Vukusic, K. Yhland, and J. Stake, "A subharmonic graphene FET mixer," *IEEE Electron Device Lett.*, vol. 33, no. 1, pp. 71–73, Jan. 2012. doi: [10.1109/LED.2011.2170655](https://doi.org/10.1109/LED.2011.2170655).
- [32] M. Bonmann, M. A. Andersson, Y. Zhang, X. Yang, A. Vorobiev, and J. Stake, "An integrated 200-GHz graphene FET based receiver," in *Proc. 43rd Int. Conf. Infr., Millim., THz Waves*, Nagoya, Japan, Sep. 2018, pp. 1–3. doi: [10.1109/IRMMW-THz.2018.8510069](https://doi.org/10.1109/IRMMW-THz.2018.8510069).
- [33] O. Habibpour, Z. S. He, W. Strupinski, N. Rorsman, T. Ciuk, P. Ciepielewski, and H. Zirath, "A W-band MMIC resistive mixer based on epitaxial graphene FET," *IEEE Microw. Wireless Compon. Lett.*, vol. 27, no. 2, pp. 168–170, Feb. 2017. doi: [10.1109/LMWC.2016.2646998](https://doi.org/10.1109/LMWC.2016.2646998).
- [34] M. A. Andersson, Y. Zhang, and J. Stake, "A 185–215-GHz subharmonic resistive graphene FET integrated mixer on silicon," *IEEE Trans. Microw. Theory Techn.*, vol. 65, no. 1, pp. 165–172, Jan. 2017. doi: [10.1109/TMTT.2016.2615928](https://doi.org/10.1109/TMTT.2016.2615928).
- [35] Y. Zhang, M. A. Andersson, and J. Stake, "A 200 GHz CVD graphene FET based resistive subharmonic mixer," in *IEEE MTT-S Int. Microw. Symp. Dig.*, San Francisco, CA, USA, May 2016, pp. 1–4. doi: [10.1109/MWSYM.2016.7540287](https://doi.org/10.1109/MWSYM.2016.7540287).
- [36] A. Hamed, O. Habibpour, M. Saeed, H. Zirath, and R. Negra, "W-band graphene-based six-port receiver," *IEEE Microw. Wireless Compon. Lett.*, vol. 28, no. 4, pp. 347–349, Apr. 2018. doi: [10.1109/LMWC.2018.2808416](https://doi.org/10.1109/LMWC.2018.2808416).
- [37] A. A. Generalov, M. A. Andersson, X. Yang, A. Vorobiev, and J. Stake, "A heterodyne graphene FET detector at 400 GHz," in *Proc. 42nd Int. Conf. Infr., Millim., THz Waves*, Cancun, Mexico, Aug./Sep. 2017, pp. 1–2. doi: [10.1109/IRMMW-THz.2017.8067234](https://doi.org/10.1109/IRMMW-THz.2017.8067234).
- [38] S. Ver Hoeye, A. I. Hadarig, C. Vázquez, M. Fernández, L. Alonso, and F. Las-Heras, "Submillimeter wave high order frequency multiplier based on graphene," *IEEE Access*, vol. 7, pp. 26933–26940, 2019. doi: [10.1109/ACCESS.2019.2901577](https://doi.org/10.1109/ACCESS.2019.2901577).
- [39] A. Hadarig, S. Ver Hoeye, C. Vázquez, M. Fernández, G. Hotopan, R. Camblor, and F. Las Heras, "7th order sub-millimeter wave frequency multiplier based on graphene implemented using a microstrip transition between two rectangular waveguides," in *Proc. Int. Conf. Electromagn. Adv. Appl.*, Palm Beach, The Netherlands, Aug. 2014, pp. 757–760. doi: [10.1109/ICEAA.2014.6903958](https://doi.org/10.1109/ICEAA.2014.6903958).
- [40] A. I. Hadarig, S. Ver Hoeye, M. Fernández, S. Mikhailov, C. Vázquez, L. Alonso, and F. Las-Heras, "On the development of a simulation strategy to model the behavior of graphene-based devices in electromagnetic simulators," *IEEE Access*, vol. 7, pp. 74111–74121, 2019. doi: [10.1109/ACCESS.2019.2920518](https://doi.org/10.1109/ACCESS.2019.2920518).
- [41] A. I. Hadarig, C. Vázquez, M. Fernández, S. Ver Hoeye, G. R. Hotopan, R. Camblor, and F. Las-Heras, "Experimental analysis of the high-order harmonic components generation in few-layer graphene," *Appl. Phys. A: Solids Surf.*, vol. 118, no. 1, pp. 83–89, 2015. doi: [10.1007/s00339-014-8739-y](https://doi.org/10.1007/s00339-014-8739-y).
- [42] C. V. Antuña, A. I. Hadarig, S. Ver Hoeye, M. F. García, R. C. Díaz, G. R. Hotopan, and F. L. H. Andrés, "High-order subharmonic millimeter-wave mixer based on few-layer graphene," *IEEE Trans. Microw. Theory Techn.*, vol. 63, no. 4, pp. 1361–1369, Apr. 2015. doi: [10.1109/TMTT.2015.2403854](https://doi.org/10.1109/TMTT.2015.2403854).
- [43] C. Vázquez, A. Hadarig, S. Ver Hoeye, M. Fernández, R. Camblor, G. Hotopan, and F. Las Heras, "Millimetre wave subharmonic mixer based on graphene," in *Proc. Int. Telecommun. Symp.*, Sao Paulo, Brazil, Aug. 2014, pp. 1–5. doi: [10.1109/ITS.2014.6948016](https://doi.org/10.1109/ITS.2014.6948016).
- [44] C. Vázquez, A. Hadarig, S. Ver Hoeye, R. Camblor, M. Fernández, G. Hotopan, L. Alonso, and F. Las Heras, "Millimetre wave transmitter based on a few-layer graphene frequency multiplier," in *Proc. 45th Eur. Microw. Conf.*, Paris, France, Sep. 2015, pp. 510–513. doi: [10.1109/EuMC.2015.7345812](https://doi.org/10.1109/EuMC.2015.7345812).
- [45] C. Vázquez, A. Hadarig, S. Ver Hoeye, R. Camblor, M. Fernández, G. Hotopan, L. Alonso, and F. Las Heras, "Millimetre wave receiver based on a few-layer graphene WR-5 band subharmonic mixer," in *Proc. Global Symp. Millim.-Waves*, Montreal, QC, Canada, May 2015, pp. 1–3. doi: [10.1109/GSMM.2015.7175433](https://doi.org/10.1109/GSMM.2015.7175433).
- [46] A. I. Hadarig, S. Ver Hoeye, C. Vázquez, R. Camblor, M. Fernández, G. Hotopan, L. Alonso, and F. Las Heras, "3D printed millimeter wave receiver integrating a graphene subharmonic mixer and a diagonal horn antenna," in *Proc. Global Symp. Millim.-Waves (GSMM)*, Montreal, QC, Canada, May 2015, pp. 1–3. doi: [10.1109/GSMM.2015.7175434](https://doi.org/10.1109/GSMM.2015.7175434).
- [47] S. A. Mikhailov, "Non-linear electromagnetic response of graphene," *Europhys. Lett.*, vol. 79, no. 2, Jun. 2007, Art. no. 27002. doi: [10.1209/0295-5075/79/2/27002](https://doi.org/10.1209/0295-5075/79/2/27002).
- [48] S. A. Mikhailov and K. Ziegler, "Nonlinear electromagnetic response of graphene: Frequency multiplication and the self-consistent-field effects," *J. Phys., Condens. Matter*, vol. 20, Aug. 2008, Art. no. 384204. doi: [10.1088/0953-8984/20/38/384204](https://doi.org/10.1088/0953-8984/20/38/384204).
- [49] M. M. Glazov and S. D. Ganichev, "High frequency electric field induced nonlinear effects in graphene," *Phys. Rep.*, vol. 535, no. 3, pp. 101–138, 2014. doi: [10.1016/j.physrep.2013.10.003](https://doi.org/10.1016/j.physrep.2013.10.003).
- [50] S. A. Mikhailov, "Nonperturbative quasiclassical theory of the nonlinear electrodynamic response of graphene," *Phys. Rev. B, Condens. Matter*, vol. 95, Feb. 2017, Art. no. 085432. doi: [10.1103/PhysRevB.95.085432](https://doi.org/10.1103/PhysRevB.95.085432).
- [51] M. Dragoman, A. Cismaru, A. Dinescu, D. Dragoman, G. Stavriniadis, and G. Konstantinidis, "Enhancement of higher harmonics in graphene-based coupled coplanar line microwave multipliers," *J. Appl. Phys.*, vol. 114, Oct. 2013, Art. no. 154304. doi: [10.1063/1.4825133](https://doi.org/10.1063/1.4825133).
- [52] M. Dragoman, D. Neculoiu, G. Deligeorgis, G. Konstantinidis, D. Dragoman, A. Cismaru, A. A. Muller, and R. Plana, "Millimeter-wave generation via frequency multiplication in graphene," *Appl. Phys. Lett.*, vol. 97, Aug. 2010, Art. no. 093101. doi: [10.1063/1.3483872](https://doi.org/10.1063/1.3483872).
- [53] J. J. Dean and H. M. van Driel, "Graphene and few-layer graphite probed by second-harmonic generation: Theory and experiment," *Phys. Rev. B, Condens. Matter*, vol. 82, Sep. 2010, Art. no. 125411. doi: [10.1103/PhysRevB.82.125411](https://doi.org/10.1103/PhysRevB.82.125411).
- [54] A. Y. Bykov, T. V. Murzina, M. G. Rybin, and E. D. Obraztsova, "Second harmonic generation in multilayer graphene induced by direct electric current," *Phys. Rev. B, Condens. Matter*, vol. 85, Mar. 2012, Art. no. 121413(R). doi: [10.1103/PhysRevB.85.121413](https://doi.org/10.1103/PhysRevB.85.121413).
- [55] N. Kumar, J. Kumar, C. Gerstenkorn, R. Wang, H.-Y. Chiu, A. L. Smith, and H. Zhao, "Third harmonic generation in graphene and few-layer graphite films," *Phys. Rev. B, Condens. Matter*, vol. 87, Mar. 2013, Art. no. 121406(R). doi: [10.1103/PhysRevB.87.121406](https://doi.org/10.1103/PhysRevB.87.121406).

- [56] S.-Y. Hong, J. I. Dadap, N. Petrone, P.-C. Yeh, J. Hone, and R. M. Osgood, Jr., "Optical third-harmonic generation in graphene," *Phys. Rev. X*, vol. 3, Jun. 2013, Art. no. 021014. doi: [10.1103/PhysRevX.3.021014](https://doi.org/10.1103/PhysRevX.3.021014).
- [57] R. Cambor, S. Ver Hoeye, G. Hotopan, C. Vázquez, M. Fernández, F. Las Heras, P. Álvarez, and R. Menéndez, "Microwave frequency tripler based on a microstrip gap with graphene," *J. Electromagn. Waves Appl.*, vol. 25, nos. 14–15, pp. 1921–1929, 2011. doi: [10.1163/156939311798072090](https://doi.org/10.1163/156939311798072090).
- [58] G. R. Hotopan, S. Ver-Hoeye, C. Vazquez-Antuna, R. Cambor-Diaz, M. Fernández-García, F. L. Heras Andres, P. Alvarez, and R. Menéndez, "Millimeter wave microstrip mixer based on graphene," *Prog. Electromagn. Res.*, vol. 118, pp. 57–69, Aug. 2011. doi: [10.2528/PIER11051709](https://doi.org/10.2528/PIER11051709).
- [59] G. R. Hotopan, S. Ver-Hoeye, C. Vazquez-Antuna, A. Hadarig, R. Cambor-Diaz, M. Fernández-García, and F. L. H. Andres, "Millimeter wave subharmonic mixer implementation using graphene film coating," *Prog. Electromagn. Res.*, vol. 140, pp. 781–794, Aug. 2013. doi: [10.2528/PIER13042408](https://doi.org/10.2528/PIER13042408).
- [60] N. L. Rangel, A. Gimenez, A. Sinitskii, and J. M. Seminario, "Graphene signal mixer for sensing applications," *J. Phys. Chem. C*, vol. 115, pp. 12128–12134, Jun. 2011. doi: [10.1021/jp202790b](https://doi.org/10.1021/jp202790b).
- [61] S. Groiss, I. Bardi, O. Biro, K. Preis, and K. R. Richter, "Parameters of lossy cavity resonators calculated by the finite element method," *IEEE Trans. Magn.*, vol. 32, no. 3, pp. 894–897, May 1996. doi: [10.1109/20.497385](https://doi.org/10.1109/20.497385).



ANDREEA IOANNA HADARIG received the B.Sc. degree in telecommunication engineering from the Technical University of Cluj-Napoca, Romania, in 2012, and the M.Sc. degree in information technology and mobile communications and the Ph.D. degree from the University of Oviedo, Spain, in 2013 and 2017, respectively. Since 2012, she has been a Research Assistant with the Signal Theory and Communications Group, University of Oviedo. Her research interests include design, optimization, and analysis of passive devices using waveguides and microstrip technology operating in the millimeter/submillimeter-wave, and THz frequency bands.



SAMUEL VER HOEYE received the M.Sc. degree in electronics engineering from the University of Ghent, Ghent, Belgium, in 1999, and the Ph.D. degree from the University of Cantabria, Santander, Spain, in 2002. He is currently an Associate Professor with the Department of Electrical and Electronic Engineering, University of Oviedo, Gijón, Spain. His research interests include design and analysis of microwave, millimeter wave, and THz circuits and systems. Among these are the multi-functional oscillator-based circuits and antennas, frequency scanning antennas, graphene-based frequency multipliers and mixers, imaging systems, and textile-integrated high-frequency components.



MIGUEL FERNÁNDEZ received the M.Sc. degree in telecommunication engineering, the M.Sc. degree in information technology and mobile communications, and the Ph.D. degree from the University of Oviedo, Gijón, Spain, in 2006, 2010, and 2010, respectively. From 2006 to 2008, he was a Research Fellow with the Signal Theory and Communications Group, University of Oviedo, where he has been an Associate Professor, since September 2008. His research interests include nonlinear analysis and optimization techniques for the design of oscillator-based circuits, active antennas and frequency multipliers and mixers at the microwave, millimeter/submillimeter-wave, and terahertz frequency bands.



CARLOS VÁZQUEZ received the M.Sc. degree in telecommunication engineering, the M.Sc. degree in information technology and mobile communications, and the Ph.D. degree from the University of Oviedo, Gijón, Spain, in 2007, 2008, and 2013, respectively. From 2007 to 2012, he was a Graduate Research Assistant with the Signal Theory and Communications Group, University of Oviedo, where he has been a Research Fellow, since 2012. His research interests include nonlinear analysis and optimization techniques for the design of multifunctional oscillator-based circuits, active antennas and passive components, such as frequency multipliers and harmonic mixers at microwave, millimeter/submillimeter-wave, and terahertz frequencies.



LETICIA ALONSO received the M.Sc. degree in telecommunication engineering from the University of Oviedo, Gijón, Spain, in 2014, the M.Sc. degree in systems and control engineering from the National University of Distance Learning (UNED) and the Universidad Complutense de Madrid, Spain, in 2018, and the Ph.D. degree from the University of Oviedo, in 2018, where she has been a Researcher with the Signal Theory and Communications Group, since 2014. She was a Visiting Scholar with the George Green Institute for Electromagnetics Research, University of Nottingham, U.K., in 2017. Her research interests include design, simulation, and manufacturing techniques to develop microwave and millimeter-wave passive circuits and antennas fully integrated in textile technology.



FERNANDO LAS-HERAS received the M.S. and Ph.D. degrees in telecommunication engineering from the Technical University of Madrid (UPM), in 1987 and 1990, respectively. He was a National Graduate Research Fellow and an Associate Professor with the Department of Signal, Systems and Radiocom, UPM, from 1988 to 1990 and from 1991 to 2000, respectively. From 2004 to 2008, he was the Vice-Dean of telecommunication engineering with the Technical School of Engineering, Gijón. He has been a Full Professor with the University of Oviedo, since 2003, where he has also been the Head of the Research Group: Signal Theory and Communications (TSC-UNIOVI), Department of Electrical Engineering, since 2001. He is currently a Visiting Researcher with Syracuse University, New York, a Visiting Lecturer with the National University of Engineering, Lima, and with the ESIGELEC, France. He has authored over 450 technical journals and conference papers in the areas of electromagnetic radiation, propagation and scattering theory and applications as well as inverse problems. He was a member of the Board of Directors of the IEEE Spain section, from 2012 to 2015, a member of the Board of the IEEE Microwaves and Antennas Propagation Chapter (AP03/MTT17), from 2016 to 2018, and a member of the Science, Technology and Innovation Council of Asturias, Spain, in 2010. He held the Telefónica Chair on RF Technologies, ICTs applied to environment and climate change, and ICTs and Smartcities, from 2005 to 2015.

...